

Defects in vertically vibrated monolayers of cylinders

Miguel González-Pinto,¹ Johannes Renner,² Daniel de las Heras,^{2,*} Yuri Martínez-Ratón,^{3,†} and Enrique Velasco^{4,‡}

¹*Departamento de Física Teórica de la Materia Condensada,
Universidad Autónoma de Madrid, E-28049, Madrid, Spain*

²*Theoretische Physik II, Physikalisches Institut, Universität Bayreuth, D-95440 Bayreuth, Germany*

³*Grupo Interdisciplinar de Sistemas Complejos (GISC), Departamento de Matemáticas,
Escuela Politécnica Superior, Universidad Carlos III de Madrid,
Avenida de la Universidad 30, E-28911, Leganés, Madrid, Spain*

⁴*Departamento de Física Teórica de la Materia Condensada,
Instituto de Física de la Materia Condensada (IFIMAC) and Instituto de Ciencia de Materiales Nicolás Cabrera,
Universidad Autónoma de Madrid, E-28049, Madrid, Spain*

(Dated: January 28, 2019)

We analyse liquid-crystalline ordering in vertically vibrated monolayers of cylinders confined in a circular cavity. Short cylinders form tetratic arrangements with C_4 symmetry. This symmetry, which is incompatible with the geometry of the cavity, is restored by the presence of four point defects with total topological charge +4. Equilibrium Monte Carlo simulations predict the same structure. A new method to measure the elastic properties of the tetratic medium is developed which exploits the clear similarities between the vibrated dissipative system and the thermal equilibrium system. Our observations open up a new avenue to investigate the formation of defects in response to boundary conditions, an issue which is very difficult to realize in colloidal or molecular systems.

Monolayers of vertically-vibrated grains have been shown to exhibit a surprisingly rich behaviour [1–5], including pattern formation in steady-state structures and non-equilibrium phenomena [6]. Even though experimental control parameters, such as vibration frequency and amplitude, critically affect the observed phenomena, in some regions of parameter space non-equilibrium behaviour is absent or not predominant, and observed patterns resemble those typical of interacting particle systems in thermal equilibrium. Of particular interest are the patterns exhibited by elongated particles with cylindrical shape, which project on a plane approximately as hard rectangles (HR); when their aspect ratio is moderate, these particles arrange into two-dimensional monolayers with strong tetratic correlations [1, 7, 8]. The tetratic phase is a liquid-crystalline arrangement with particles aligned preferentially along two equivalent perpendicular orientations with global C_4 symmetry. Mean-field density-functional theories for rectangular particles in thermal equilibrium had predicted the existence of this phase [9, 10], which was confirmed experimentally [11] and by simulation [12, 13]. It is remarkable that the same symmetry has also been observed in monolayers of vibrated granular rods [1, 7, 8]. Some theoretical ideas have been advanced to explain general similarities between thermal and granular systems [4, 14], but none of them is based on deep physical roots. In the case of systems exhibiting liquid-crystalline order only plausible mechanisms that drive locally ordered arrangements of particles can be invoked [8]. Also, from the experimental evidence, it is tempting to use arguments based on equilibrium entropy maximisation and excluded-volume ideas to qualitatively explain the effective driving forces that lead to the extended ordered domains observed in the non-equilibrium vibrated granular systems, like in the

corresponding equilibrium fluid of two-dimensional HR.

Before a complete theoretical framework for vibrated granular two-dimensional particles is formulated, more evidence on their similarities with thermal particles is building up. In our previous paper [8], we briefly reported on a yet another intriguing behaviour of vibrated granular matter, this time in a monolayer of cylinders contained in a quasi-two-dimensional circular cavity. We showed that the tetratic monolayer exhibits four defects symmetrically located at the corners of a square.

In the present paper we analyse this experimental system in detail and show that this behaviour is exactly what is expected in an equivalent thermal system: our Monte Carlo (MC) simulations of such a system give rise to exactly the same structure [15]. Therefore the granular monolayer can respond to geometrical frustration much like what one would expect in a thermal system, i.e. by creating localised defects that interact through the elastic stiffness of the fluid tetratic medium. Also, we show that the defected structure is stable in time and occurs in a range of densities. Finally, we propose a method to calculate the effective interaction between defects in an equilibrium system, and from this the elastic stiffness modulus of the liquid-crystal medium. Assuming that the granular system can be treated in the same manner, the resulting modulus turns out to be of the same order of magnitude in both thermal and granular systems. Our conclusion is that not only their local order and their response to geometric frustration in terms of defect formation are similar, but also that the elastic properties that mediate long-range interactions between the defects are similar.

From the evidence gathered by previous experiments [1, 7, 8], it is clear that the configurations of cylinders of low length (L)-to-width (D) ratio $\kappa = L/D$ change,

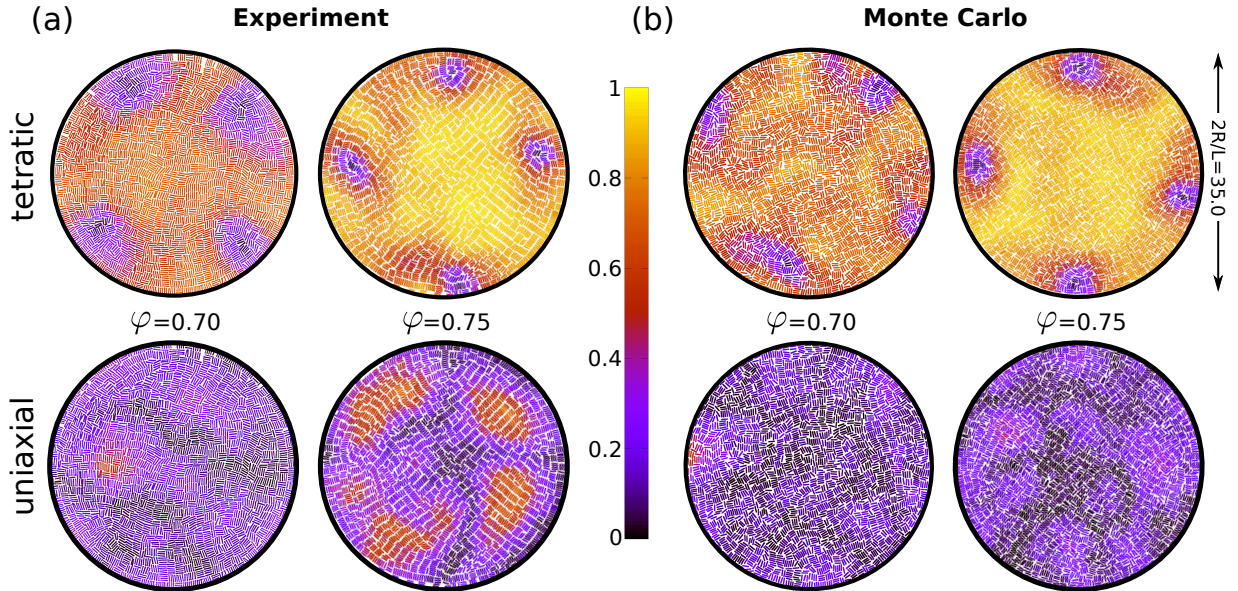


FIG. 1: Colour maps of the local tetratic q_4 and uniaxial q_2 order parameters. The colour of each particle represents the value of the order parameter as specified in the central colour bar. Data for the cases $\varphi = 0.70$ and 0.75 , $\kappa = 4$ and $2R/L = 35.0$ from (a) the experiment, and (b) MC simulation. Particles have been slightly shortened to improve visualization, and holes in (a) correspond to particles that could not be identified by the imaging software.

as packing fraction $\varphi = \rho LD$ (where $\rho = N/A$ is the effective density, with N the number of cylinders and A the area) is increased, from orientationally disordered, or *isotropic*, fluid arrangements, to *tetratic* fluid configurations. Tetratic configurations persist for aspect ratios up to $\kappa \simeq 7$; this limit is also predicted by Monte Carlo (MC) simulations of HR in thermal equilibrium [7] and supported by density-functional theories [16]. At even higher densities smectic fluctuations can also be seen in the experiment [8].

Experiment

In the experiment (see Ref. [8] for more details) cylinders made of nonmagnetic steel with length 4 mm and width 1 mm ($\kappa = L/D = 4$) are placed inside a horizontal circular cavity made of aluminium and covered from above by a circular methacrylate lid resulting in a free height of 1.8 mm and radius $R = 7$ cm ($R/L = 17.5$). The sample is mechanically agitated using an electromagnetic shaker which generates a sine-wave vertical motion of frequency $\nu = 37$ Hz and amplitude a_0 with an effective acceleration $\Gamma = 4\pi^2 a_0 \nu / g \simeq 2$, with g the gravity's acceleration. The images were taken with a carefully collimated digital camera during the whole duration of the experiment (roughly 3 hours).

Particle identification (position and orientation) is done using the ImageJ [17] software supplemented by our own image processing code. Three types of particle arrangements are observed: isotropic, where particles are disordered in both orientations and positions; tetratic, where particles show fluid behaviour but are oriented on

average along two equivalent, perpendicular directions; and smectic, with particles forming fluid layers. These configurations are identified by means of order parameters $q_n = \langle \cos n\vartheta \rangle$, with $n = 2, 4$ (respectively uniaxial and tetratic order parameters), and $q_s = \langle e^{i\mathbf{q}\cdot\mathbf{r}} \rangle$ (smectic order parameter) on each particle, where ϑ is the angle of the particle with respect to the local alignment direction $\hat{\mathbf{n}}$, \mathbf{r} its position and \mathbf{q} a wavevector compatible with the cylinder length. In locally tetratic configurations $q_2 < q_4$ and $q_s \sim 0$; isotropic and smectic configurations are identified by $q_2 \sim q_4 \sim 0$, $q_s \simeq 0$ and $q_2 > q_4$, $q_s > 0$, respectively. Note that, in our experiments, extended uniaxial nematic configurations are not formed for any value of aspect ratio and, due to geometric frustration and excitation of vorticity smectic domains are limited in size and time [8].

Simulation

Two types of simulations have been performed in this work. First, we conducted equilibrium MC simulations on a system of HR that intends to mimic the experimental granular system, i.e. using the same particle aspect ratio, cavity radius and packing fraction. Each particle is characterized by its position and orientation vector. N particles are placed in cavity of radius $R/L = 17.5$. The interaction between the particles and the cavity is a hard potential acting on the corners of the particles. That is, the wall-particle potential is infinity if at least one corner of the particle is outside the cavity and vanishes otherwise.

Following the ideas of Ref. [18] we initialize the sys-

tem at very low packing fraction $\varphi = 0.1$ for which the equilibrium state is isotropic. Next we adiabatically increase the number of particles in steps of $\Delta\varphi = 0.05$ until the desired packing fraction is reached. After every increment in the number of particles we run 10^6 Monte Carlo Sweeps (MCS) to equilibrate the system. Each MCS is an attempt to sequentially move and rotate every particle in the system. The maximum rotation and displacement each particle is allowed to perform in one MCS is recalculated in each simulation such that the acceptance probability of the motion is ~ 0.25 . In order to insert new particles we randomly select one particle in the cavity and create a replica with the same orientation but displaced by $\sim D$ along the long axis. If the new particle overlap with other particles or with the cavity we reject the insertion and select another random particle. Once a new particle is accepted we perform a few hundred rotations and translations on it. The orientational order parameters and other quantities of interest, such as the positions of the defects, are calculated following the same procedures as for the experiments.

Second, we performed Brownian simulations on systems of four point particles inside a circular cavity. These effective particles represent point defects of the real system. The effective particles interact with each other via a repulsive pair potential $u(s) = -c \log(s/a)$, where a is an irrelevant length-scale, s is the interdefect distance, and c is a strength parameter related to the stiffness coefficient. The use of a logarithmic pair potential can be justified by invoking the interaction that results from the solution of the Frank elastic theory [19]. In the elastic theory the constant a is the characteristic dimension of the defect core. However at the dynamical level this constant does not play any role because forces are not affected by its value. Therefore we used $a = R$ as a length-scale. In addition, the effect of the cavity surface is introduced through a potential $V(r) = \epsilon \exp[-\lambda(R-r)]$, where ϵ , and λ are the strength and the inverse decay-length of the wall potential. Defects are assumed to be subject to thermal fluctuations from particles in the tetratic medium, driven by a thermal energy $k_B T$. These fluctuations are taken care of by solving a Langevin equation $m\dot{\mathbf{v}}_i = \mathbf{F}_i - \zeta\mathbf{v}_i + \mathbf{g}_i$, where m is an effective mass, \mathbf{v}_i the velocity of the i th defect, \mathbf{F}_i the force on the defect from the total potential $V(r_i) + \sum_{j \neq i} u(r_{ij})$, ζ a friction coefficient, and \mathbf{g}_i a stochastic white noise. Using the cavity radius R and the parameter c as length and energy scales, respectively, the dimensionless discretised equation, in the non-inertial, Brownian regime, becomes

$$\mathbf{r}_i^*(t+h) = \mathbf{r}_i^*(t) + \gamma \mathbf{F}_i^*(t) + \sqrt{2\gamma T^*} \boldsymbol{\eta}_i(t), \quad (1)$$

where $\mathbf{r}_i^*(t)$ is the position of the i th defect in units of R at time t , \mathbf{F}_i^* is the force on the i th defect in units of c/R , $T^* = k_B T/c$, where T is an effective temperature, $\gamma = hc/R^2\zeta$, h the time step, and $\boldsymbol{\eta}_i$ a dimensionless

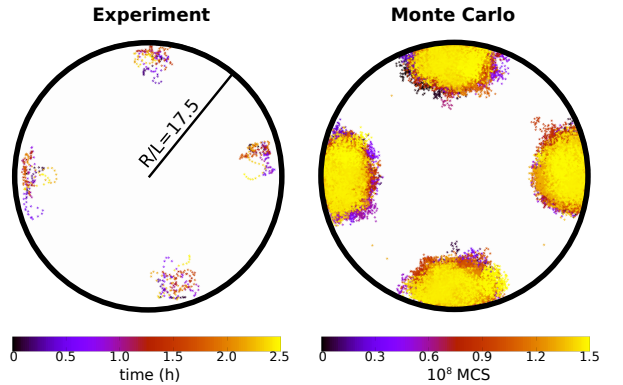


FIG. 2: Sampling of defect positions in experiment (left) and Monte Carlo simulation (right). Colour bars below indicate the experimental time in hours, and the ‘MC time’ in units of 10^8 MC sweeps.

Gaussian noise of unit variance and zero mean. The free parameters of the model are T^* , $\lambda^* = \lambda R$, and $\epsilon^* = \epsilon/c$. Since the simulations involve only four particles they can be extended for several hundred millions time steps to collect statistically significant information.

Fig. 1 shows particle configurations from (a) our experiment and (b) Monte Carlo simulation. In each case two values of the packing fraction, $\varphi = 0.70$ and 0.75 , are shown. The two orientational order parameters, uniaxial q_2 and tetratic q_4 , have been coded in false colour on each particle, using the same protocols in both experiment and simulation. To obtain the order parameter fields at some point \mathbf{r} we average over the particles located within a circular region of radius $\xi = 4L$ centered at \mathbf{r} as discussed in Ref. [8].

The structure in the cavity is similar in the two cases, experiment and thermal model. Also, tetratic configurations are visible at the two densities, as indicated by the high values of the tetratic order parameter (see central colour bar) and the low values of the uniaxial order parameter. In these ‘fluid’ configurations, which are very stable, particles are globally oriented along two perpendicular directions, with approximately half of the particles pointing in each direction. This balance holds locally, except in the high-density experimental configuration shown, which exhibits clear patches where the q_2 order parameter is enhanced; these correspond to domains where particles point along a common direction and organise into ‘smectic’ layers. Smectic domains fluctuate in time in a sea of particles with tetratic order. When present, as in the configuration shown, they adopt a four-fold symmetry. In the q_4 maps four regions containing particles with a q_4 -depleted neighbourhood are also clearly visible. These regions are always present in this range of densities. They can be assimilated to point

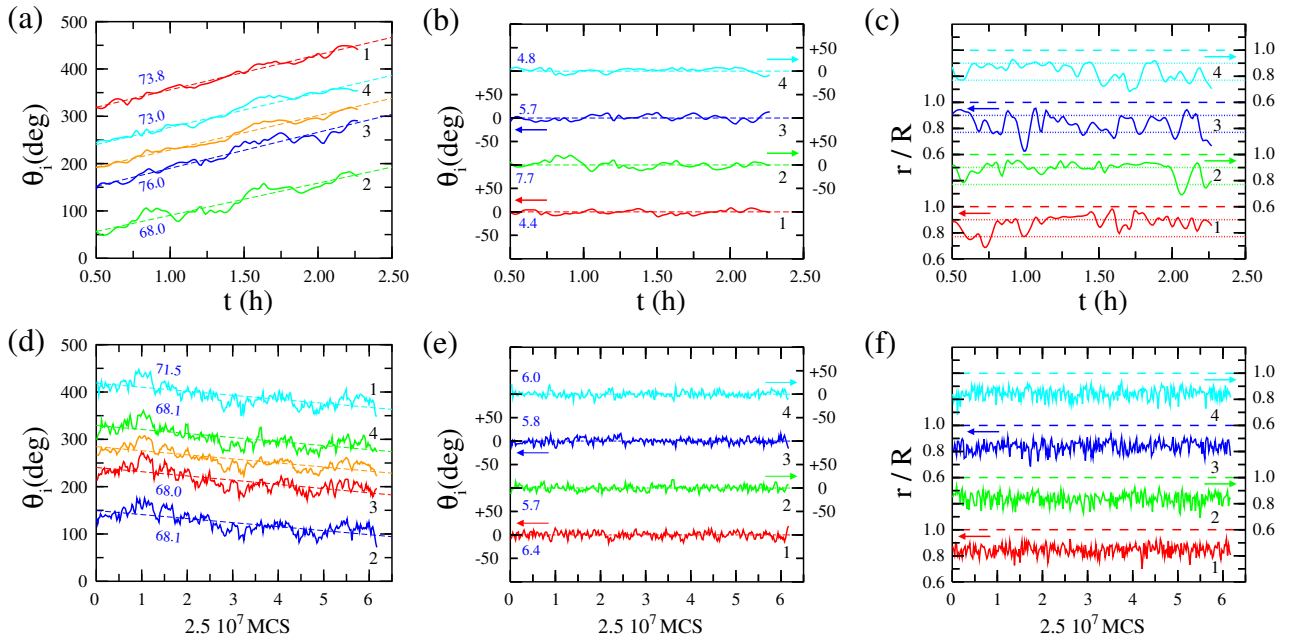


FIG. 3: (a)-(c) Experimental positions of the four defects as a function of time (given in hours). Data for each defect are displaced for clarity. (a) Azimuthal angles θ_i in the lab frame for each defect (indicated as labels). The average angle is represented by the orange curve. Dashed lines are linear fits, while labels in blue indicate the values of the slope in degrees per hour. (b) Same as in (a), but angles referred to the instantaneous rotating frame (curve in orange in panel (a)). Labels indicate variance in each case. (c) Defect radial distances r/R scaled with cavity radius. Dashed lines indicate the edge of the cavity in each case, while dotted lines correspond to the two maxima of radial distance distribution, Fig. 4(b). Panels (d)-(f) show the same magnitudes as obtained from MC simulations. In (d) labels indicate the absolute value of the slope in degrees per MCS, multiplied arbitrarily by a factor 2×10^8 to make it of the same order of magnitude as in panel (a).

defects of topological charge $\mathcal{Q}_i = +1$ ($i = 1, \dots, 4$). The presence of these four defects restores the globally tetratic symmetry, which is broken by the circular geometry of the cavity. The total charge $+4$ satisfies the constraint imposed by the Gauss-Bonnet theorem for a medium with C_4 symmetry. Note that these numbers fulfill the equation $\sum_i \mathcal{Q}_i = p\chi$, with $p = 4$ the p -fold symmetry of the tetratic phase, while $\chi = 1$ is the Euler characteristic of the disk [19]. The same four-defect structure is visible in the MC simulations. Indeed the thermal system reacts to confinement in the same way as the granular system, i.e. by creating four point defects symmetrically located next to the wall. In this case, however, smectic domains are never seen; instead, the whole cavity is filled with a defected smectic configuration at higher densities (not shown). By comparing the uniaxial and tetratic maps for density $\varphi = 0.75$, Fig. 1(a), we can see that the smectic domains in the experiments at high densities are located between neighbouring defects and close to the wall. As shown in our previous work, the presence of smectic textures at high packing fractions in granular rods with relative small aspect ratio is due to strong particle clustering promoted by a local energy dissipation mechanism [8].

In order to understand the similarities and differences

between the two systems in more detail, we have analysed the average defect behaviour. First we computed the position $\mathbf{r} = (x, y)$ of the point defects using the q_4 order parameter by identifying those particles with $q_4 < 0.2$; in strongly-developed tetratic configurations such as the ones shown in Fig. 1. This protocol leads to four well-separated groups of particles associated with each of the four regions where the tetratic order is depleted. The centre of mass of each group of particles, \mathbf{r} , is taken as the position of the corresponding defect. The same procedure is implemented in both experiments and MC simulation.

In the following the lab frame is assumed to be placed at the centre of the circular cavity, and polar coordinates $\mathbf{r} = (r \cos \theta, r \sin \theta)$ for the position of the defects are used to analyse various trends and distributions. The unwanted tendency of the system to rotate [20], both in experiments and simulations, is suppressed by calculating the instantaneous average of the azimuthal angle over the four defects and subtracting this angle from the angular position of each defect. This process isolates the inherent fluctuations of the defects about a mean position by referring their motion to a frame that rotates rigidly with the sample. Fig. 2 shows the sampled positions of the defects in this frame for both systems at packing fraction $\varphi = 0.75$ (in the following results are presented

only for this case, since all the densities explored, in the range $\varphi = 0.70 - 0.75$, are qualitatively similar, while for $\varphi > 0.75$ large clusters in smectic-like configurations strongly compete with the tetratic ordering). Defects are colour-coded according to either the experimental time or the ‘MC time’. The plot shows that the system is being sampled ergodically. Sampling in the experimental system is comparatively poorer.

The time evolution of defect positions in the experiment and in the MC simulation are shown in detail in Fig. 3. Panels (a)-(c) correspond to the experiment, while panels (d)-(f) show the MC results. Fig. 3(a) shows the time evolution of the defect angles θ_i , $i = 1, \dots, 4$, and also of the average angle with respect to the lab frame. In this particular experiment the sample rotates globally in one direction, but this is not the case in general. Clearly defects slowly rotate with approximately constant angular velocity ω and with superimposed fluctuations. Particle tracking and velocity calculations indicate that this rotation is very rigid (i.e. linear velocity is roughly proportional to radial distance). Some of these fluctuations are correlated, meaning that the solid-body rotation occurs at nonconstant angular velocity $\omega(t)$.

Fig. 3(b) shows the angles θ_i with respect to the frame with axes rotating with $\omega(t)$; in this frame individual defect fluctuations about their mean are isolated and can be properly analysed. The radial distance of the defects also fluctuates in time, Fig. 3(c). In general defects stay close to the surfaces, which results from the repulsive defect interactions (we further comment on this point below). MC simulation results, shown in Figs. 3(d)-(f), are qualitatively similar. Note that the poorer experimental sampling due to practical time restrictions limit the temporal extent of fluctuations with respect to the simulation.

To show the fluctuation dynamics of the defects in more detail, the distribution of azimuthal angle, $f(\theta)$, is plotted in Fig. 4(a). Defect libration closely follows a Gaussian distribution in both systems, but the MC result presents a slightly broader distribution, although this is not conclusive due to the relatively poorer statistics in the experiment. The radial distance distributions $f_1(r)$ in the granular and thermal systems are also qualitatively similar, see Fig. 4(b). They are not Gaussian but bimodal. In the case of the experiment this is clearly seen in Fig. 3(c), where the position of the two favoured distances is indicated by horizontal dotted lines. Our interpretation for the bimodality is the following: even though defects repel each other, particles do form an ordered surface structure that modifies the wall-defect interaction and prevents defects from reaching the wall. However, when this surface layer is absent, defects can be in close contact with the surface, resulting in the existence of two favoured distances from the wall. The thickness of the surface layer is mainly determined by the density, but it differs substantially in the experiment and MC simu-

lations, since the favoured particle surface orientation is different. In the experiment, the orientation is mostly along the wall normal, with a thickness of one or two particle lengths. In the MC simulations, by contrast, the orientation is mostly planar [18], with a thickness of a few particle widths. In both cases the average defect position along the radial distance is determined by the competition between the repulsive defect-defect interaction, which tends to push the defects to the wall, and the repulsive surface-defect interaction, which depends on the particle orientation at the wall. The final distribution is bistable, but the location of the two maxima is different in the experiment and in the MC simulation because of the different particle orientation favoured at the wall.

To better characterise the defect dynamics, we have also calculated the distribution of relative distances between the defects, $f_2(s)$, which is shown in Fig. 4(c). As expected, it is also bimodal and exhibits two maxima, corresponding to the nearest neighbour and next-nearest neighbour distances. The ratio between the two is very close to $\sqrt{2}$, which confirms that the defects on average form a square configuration. This arrangement is again the result of the repulsive surface-defect, and defect-defect interactions. The distribution can be regarded as a superposition of two distributions located at the two characteristic distances.

The similarities between the MC simulations and the granular experiment shown above as regards the distribution functions f_i suggests that the nonequilibrium fluctuations of the order-parameter field in the experimental system can be assimilated to that of an effective system of Brownian point defects interacting through a fluctuating elastic medium. The medium would be characterised by means of an elastic constant. The mapping is natural for the equilibrium MC simulation. However, in the case of the experiment this mapping is not clear. The connection can be realised by relating the fluctuations of the order-parameter field in the experiment, scaled with an effective temperature, to that of the equilibrium system, measured through the usual elastic constant scaled with the temperature. Fluctuations in the experiment certainly depend on dissipation mechanisms such as inelastic particle interactions or friction between particles. Also, the definition of temperature in a granular system is controversial, and several choices can be found in the literature. Therefore we suggest, as a working hypothesis, that the strength of elastic interactions, scaled with an effective temperature, in the granular and equilibrium systems, are similar. We used this scaled elastic constant estimation as a way to quantify these interactions. The mapping is a mere hypothesis, and the precise value of the scaled elastic constant in the granular system might be different to that obtained below. Therefore, our result should be treated as a conjecture to be confirmed in the future by other direct methods.

We have implemented this procedure to extract in-

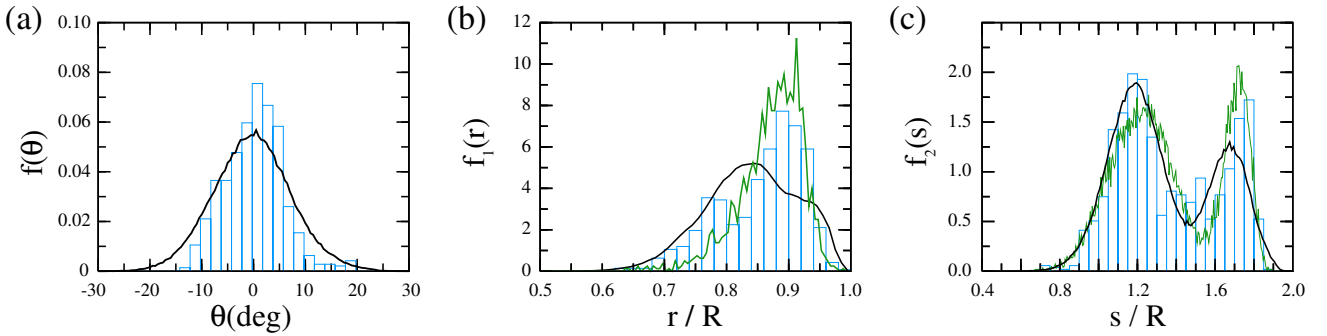


FIG. 4: (a) Azimuthal angle distribution $f(\theta)$ from experiment (histogram) and simulation (black curve). (b) Radial distance distribution $f_1(r)$ from experiment (histogram) and simulation (black curve), with respect to radial distance scaled with cavity radius. (c) Distribution of the relative distance between defects, $f_2(s)$, with respect to the interdefect distance scaled with cavity radius. Histogram: experimental results. Black curve: simulation. Green curves in (b) and (c): Brownian simulation using the best-fit method applied on $f_2(s)$, as explained in the text.

formation about the elastic stiffness coefficient of the tetratic medium. In fact, the use of elastic-theoretical concepts in the context of granular monolayers is not new. Galanis et al. [3] applied elastic theory on the global orientation field of a vibrated monolayer to infer the elastic behaviour of a monolayer consisting of very long rod in a uniaxial nematic configuration. However, defects were omitted from the analysis. Here we proceed differently, and assume the defect dynamics shown in the previous paragraphs can be modeled by equilibrium thermal fluctuations of an effective system of four Brownian particles interacting through logarithmic potentials with no intervening medium. A numerical value for the conjectured elastic stiffness coefficient K of the tetratic medium is then extracted by comparing the defect distribution of the experiment to that of the thermal effective model, explored by means of Brownian simulation.

As pointed out before, the model has three free parameters: T^* , $\lambda^* = \lambda R$, and $\epsilon^* = \epsilon/c$. To obtain their values we focus on the relative-distance distribution $f_2(s)$ and define a best-fit function in terms of the distance-integrated square difference between the experimental and the time-averaged Brownian distribution extracted from simulation with fixed parameters T^* , λ^* , ϵ^* . The values of these parameters are then optimised by minimising this function (note that the simulation results do not depend on the scaled inverse friction coefficient γ). The optimised values are $T^* \approx 0.07$, $\lambda^* \approx 25$ and $\epsilon^* \approx 1.0$.

The optimised $f_2(s)$ function is shown in green in Fig. 4(c). The fitting is reasonable. Also in Fig. 4(b) the function $f_1(s)$ from the Brownian simulation is shown in green. Despite not being used as a target function, the comparison with the experimental distribution $f_1^{(\text{exp})}(r)$ is reasonable.

From the above optimised value of the parameters we obtain $c \simeq 14 k_B T$. Since we expect the coefficient c to

be related to the elastic stiffness coefficient by $c = \pi k^2 K$ [19], where $k = 1/4$ is the winding number of each of the four $+1$ defects, we obtain the elastic stiffness coefficient as $K/k_B T \simeq 70$. We note that, to accommodate the fine structure of the experimental distribution $f_2^{(\text{exp})}(s)$, we also used a bistable wall potential $V(r)$. The resulting value for the scaled K hardly changes, even though the fit certainly improves.

It is interesting to note that the value of the scaled K obtained is remarkably close to the values of elastic coefficients in two-dimensional nematic liquid-crystal phases. A two-dimensional nematic can only support splay and bend distortions, with elastic coefficients K_1 and K_3 , respectively. In the tetratic phase symmetry imposes $K_1 = K_3 = K$. To our knowledge the only calculations of elastic constants in two-dimensional liquid crystals focused on rather long rods (which can only exhibit uniaxial nematic ordering [21]) at relatively low densities. The values have the same order of magnitude as the one obtained here. Obviously a fitting of the Brownian model to the MC $f_2(s)$ function, which should be equivalent to a direct calculation of K , gives a similar value. However we note that, in the experiment, smectic fluctuations in the regions between neighbouring defects are frequent, as can be seen in Fig. 1. This adds an extra stiffness to the effective defect interaction, a feature that could explain the differences observed in $f_2(s)$ between experiment and the equilibrium simulation.

In summary, we have shown that a vertically vibrated monolayer of granular rods can form configurations with tetratic symmetries in a circular cavity. To restore the global symmetry broken by the cavity, the system develops four localised defects close to the wall forming a square configuration. This is completely similar to the behaviour of the equivalent thermal monolayer, which we have also investigated using MC simulation. In addition, the defect fluctuations about their average positions

in the experimental and thermal systems are similar. We have exploited this observation to conjecture that a properly scaled elastic stiffness coefficient for the granular monolayer should be similar to that of the equilibrium MC simulation. In order to exploit this idea, a Brownian dynamics simulation has been used to extract a value for such a scaled elastic constant. The resulting value is close to those obtained from equilibrium theories on hard rods in two dimensions. Our results give evidence that vibrated monolayers of dissipative particles, at least in some window of experimental conditions, have similar ordering properties, respond equally to symmetry-breaking external fields, and would possess elastic stiffness constants as in the corresponding thermal systems.

The fact that the number of defects and their spatial distributions depend on the symmetry of the ordered phases (nematic, tetratic or smectic) and on the geometrical restrictions imposed by confinement, makes granular rod monolayers an ideal tool to device well controlled experiments with the aim to study the dependence of these properties on the system boundary conditions. For example the design of a ring-shaped container could change the nature of stationary textures present in the system and also the distribution of defects [22]. Note that, in experiments on colloidal or molecular systems, the presence of non-controlled heterogeneities at particle length scales in the confining surfaces gives rise to important fluctuations that distort the orientational director field and consequently the final distribution of defects. Moreover, the study of liquid-crystalline textures and defects in granular systems is not limited to quasi-two-dimensional systems [23].

Financial support under grants FIS2015-66523-P and FIS2017-86007-C3-1-P from Ministerio de Economía, Industria y Competitividad (MINECO) of Spain is acknowledged.

* Electronic address: delasheras.daniel@gmail.com

† Electronic address: yuri@math.uc3m.es

‡ Electronic address: enrique.velasco@uam.es

[1] V. Narayan, N. Menon, and S. Ramaswamy, *J. Stat. Mech. - Theory and Experiment*, P01005 (2006).

- [2] J. Galanis, D. Harries, D. L. Sackett, W. Losert, and R. Nossal, *Phys. Rev. Lett.* **96**, 028002 (2006).
- [3] J. Galanis, R. Nossal, W. Losert, and D. Harries, *Phys. Rev. Lett.* **105**, 168001 (2010).
- [4] I. S. Aranson, and L. S. Tsimring, *Rev. Mod. Phys.* **78**, 641 (2006).
- [5] E. Khain, and I. S. Aranson, *Phys. Rev. E* **84**, 031308 (2011).
- [6] V. Narayan, S. Ramaswamy, and N. Menon, *Science* **317**, 105 (2007).
- [7] T. Muller, D. de las Heras, I. Rehberg, and K. Huang, *Phys. Rev. E* **91**, 062207 (2015).
- [8] M. González-Pinto, F. Borondo, Y. Martínez-Ratón, and E. Velasco, *Soft Matter* **13**, 2571 (2017).
- [9] H. Schlacken, H.-J. Mogel, and P. Schiller, *Mol. Phys.* **93**, 777 (1998).
- [10] Y. Martínez-Ratón, E. Velasco, and L. Mederos, *J. Chem. Phys.* **122**, 064903 (2005).
- [11] K. Zhao, C. Harrison, D. Huse, W. B. Russel, and P. M. Chaikin, *Phys. Rev. E* **76**, 040401(R) (2007).
- [12] A. Donev, J. Burton, F. H. Stillinger, and S. Torquato, *Phys. Rev. B* **73**, 054109 (2006).
- [13] Y. Martínez-Ratón and E. Velasco, *Phys. Rev. E* **79**, 011711 (2009).
- [14] R. Blumenfeld, and S. F. Edwards, *Eur. Phys. J.* **223**, 2189 (2014).
- [15] These defects have also been theoretically studied by MC simulations and elastic free-energy calculations on thermal systems with tetratic ordering on spherical surfaces, resulting in the presence of eight disclinations located at the vertexes of an anticube. See Y. Li, H. Miao, H. Ma, and J. Z. Y. Chen, *Soft Matter* **9**, 11461 (2013), and O. V. Manuhina and M. J. Bowick, *Phys. Rev. Lett.* **114**, 117801 (2015).
- [16] Y. Martínez-Ratón, E. Velasco, and L. Mederos, *J. Chem. Phys.* **125**, 014501 (2006).
- [17] <https://imagej.nih.gov/ij/>
- [18] D. de las Heras and E. Velasco, *Soft Matter* **10**, 1758 (2014).
- [19] M. J. Bowick and L. Giomi, *Adv. Phys.* **58**, 449 (2009).
- [20] I. S. Aranson, D. Volfson, and L. S. Tsimring, *Phys. Rev. E* **75**, 051301 (2007).
- [21] D. de las Heras, L. Mederos, and E. Velasco, *Liq. Cryst.* **37**, 45 (2009).
- [22] I.C. Gârlea, P. Mulder, J. Alvarado, O. Damme, D.G.A.L. Aarts, M.P. Lettinga, G.H. Koenderink, and B.M. Mulder, *Nat. Commun.* **7**, 12112 (2016).
- [23] K. Asencio, M. Acevedo, I. Zuriguel, D. Maza, *Phys. Rev. Lett.* **119**, 228002 (2017).